

## Reversible Magnetism between an Antiferromagnet and a Ferromagnet Related to Solvation/Desolvation in a Robust Layered $[\text{Ru}_2]_2\text{TCNQ}$ Charge-Transfer System

Natsuko Motokawa,<sup>†</sup> Satoshi Matsunaga,<sup>†,§</sup> Shinya Takaishi,<sup>†</sup> Hitoshi Miyasaka,<sup>\*,†</sup> Masahiro Yamashita,<sup>†</sup> and Kim R. Dunbar<sup>‡</sup>

Department of Chemistry, Graduate School of Science, Tohoku University, 6-3 Aramaki-Aza-Aoba, Aoba-ku, Sendai, Miyagi 980-8578, Japan, and Department of Chemistry, Texas A&M University, P.O. Box 30012, College Station, Texas 77842-3012

Received March 22, 2010; E-mail: miyasaka@agnus.chem.tohoku.ac.jp

**Abstract:** The charge-transfer compound  $[\{\text{Ru}_2(\text{O}_2\text{CPh-}o\text{-Cl})_4\}_2\text{TCNQ}(\text{MeO})_2] \cdot \text{CH}_2\text{Cl}_2$  (**1**;  $o\text{-ClPhCO}_2^- = o\text{-chlorobenzoate}$ ;  $\text{TCNQ}(\text{MeO})_2 = 2,5\text{-dimethoxy-}7,7,8,8\text{-tetracyanoquinodimethane}$ ) was synthesized from the reaction of the neutral precursors  $[\text{Ru}_2^{\text{II,II}}(\text{O}_2\text{CPh-}o\text{-Cl})_4]$  (abbreviated as  $[\text{Ru}_2^{\text{II,II}}]$  or  $[\text{Ru}_2^{4+}]$ ) and  $\text{TCNQ}(\text{MeO})_2$  in a  $\text{CH}_2\text{Cl}_2/\text{nitrobenzene}$  solution. The structure consists of two-dimensional layers consisting of an infinite array in which  $[\text{Ru}_2^{\text{II,II}}]$  units are involved in charge transfer to  $\text{TCNQ}(\text{MeO})_2$  to give a formal charge of  $[\{\text{Ru}_2^{4.5+}\}\text{-TCNQ}(\text{MeO})_2^{\bullet-}\{\text{Ru}_2^{4.5+}\}]$ . Interstitial  $\text{CH}_2\text{Cl}_2$  molecules are located in the void spaces between the layers. Strong intralayer magnetic coupling between the units  $[\text{Ru}_2^{\text{II,II}}]$  with  $S = 1$  or  $[\text{Ru}_2^{\text{II,III}}]$  with  $S = 3/2$  and  $\text{TCNQ}(\text{MeO})_2^{\bullet-}$  with  $S = 1/2$ , as well as long-range ordering due to antiferromagnetic interlayer interactions, was observed. An antiferromagnetic ground state exists below  $T_N = 75$  K, which undergoes a metamagnetic transition under applied fields less than 2 T to a field-induced canted antiferromagnetic state with large coercivities up to  $H_c = 1.6$  T at 1.8 K. Compound **1** gradually loses the interstitial  $\text{CH}_2\text{Cl}_2$  molecule at room temperature to form a dried sample (**1-dry**) without loss of crystallinity and converts nearly reversibly back to **1** after being exposed to  $\text{CH}_2\text{Cl}_2$  vapor for 72 h (distinguished as **1'**). Interestingly, during this process there is no significant change in lattice dimensions and bond distances or angles with a volume change of only 1.2 vol %. The only discernible difference is ordering/disordering of a pendant ligand orientation, but the magnetism is dramatically altered to a ferromagnetic state with  $T_c \approx 56$  K for **1-dry**. The magnetic property changes are gradual and depend on the degree of interstitial  $\text{CH}_2\text{Cl}_2$  molecule loss with reversibility in the process of going between **1** and **1-dry**. In addition, in the case of partially desolvated crystals that have mixed domains of ferromagnetically and antiferromagnetically ordered domains for desolvated and solvated segments, respectively, the complete change to ferromagnet can also be triggered by magnetic fields even if the desolvated segments are comparatively minor compared to the solvated segments in a crystal. Surprisingly, the information of the existence of ferromagnetically ordered domains is dynamically recorded in the entire crystal after applying significant magnetic fields as if the majority of the antiferromagnetically ordered domains for solvated segments were never present.

### Introduction

Flexible molecular magnets that undergo a reversible change of their magnetic properties in response to external modulations such as light,<sup>1</sup> pressure,<sup>2</sup> electrical field,<sup>3</sup> humidity,<sup>4</sup> solvation/desolvation,<sup>5</sup> or molecular guest absorption/desorption<sup>6</sup> are one of the recent challenging targets in the field of molecular magnetism. With the exception of cases in which the spin state or electronic state of magnetic centers are directly modified by spin-crossover<sup>7</sup> and/or intramolecular charge transfer,<sup>1,8</sup> for example, most instances of magnetic changes are accompanied by significant structural changes that strongly affect bond-mediating magnetic paths or through-space interactions. Reversible structural changes with concomitant changes in magnetism

can be divided into four categories: (i) bond cleavage or bond formation, (ii) deformations of the lattice (lattice sliding, contracting/expanding, etc.), (iii) collapse/regeneration of lattice, or (iv) a combination of the first three processes. These changes occur either in a crystal-to-crystal phase or a crystal-to-amorphous phase transformation. A particularly notable example

- (1) (a) Sato, O.; Iyoda, T.; Fujishima, A.; Hashimoto, K. *Science* **1996**, *272*, 704. (b) Ohkoshi, S.; Hashimoto, K. *J. Am. Chem. Soc.* **1999**, *121*, 10591. (c) Arimoto, Y.; Ohkoshi, S.; Zhong, Z. J.; Seino, H.; Mizobe, Y.; Hashimoto, K. *J. Am. Chem. Soc.* **2003**, *125*, 9240. (d) Hozumi, T.; Hashimoto, K.; Ohkoshi, S. *J. Am. Chem. Soc.* **2005**, *127*, 3864. (e) Ohkoshi, S.; Tokoro, H.; Hozumi, T.; Zhang, Y.; Hashimoto, K.; Mathonière, C.; Bord, I.; Rombaut, G.; Verelst, M.; Cartier dit Moulin, C.; Villain, F. *J. Am. Chem. Soc.* **2006**, *128*, 270. (f) Ohkoshi, S.; Hamada, Y.; Matsuda, T.; Tsunobuchi, Y.; Tokoro, H. *Chem. Mater.* **2008**, *20*, 3048. (g) Tokoro, H.; Matsuda, T.; Nuida, T.; Moritomo, Y.; Ohoyama, K.; Dangui, E. D. L.; Boukheddaden, K.; Ohkoshi, S. *Chem. Mater.* **2008**, *20*, 423. (h) Ohkoshi, S.; Hamada, Y.; Matsuda, T.; Tsunobuchi, Y.; Tokoro, H. *Chem. Mater.* **2008**, *20*, 3048.

<sup>†</sup> Tohoku University.

<sup>‡</sup> Texas A&M University.

<sup>§</sup> Current address: Department of Chemistry, Faculty of Science, Kanagawa University, 2946 Tsuchiya, Hiratsuka, Kanagawa 259-1293, Japan.

of such behavior was reported by Veciana et al., who observed a reversible solvent-induced “shrinking-breathing” process in a crystal of Cu<sup>II</sup>-radical nonporous magnetic material involving large volume changes of >30 vol % that strongly influence the magnetic properties.<sup>5b</sup> Such materials were dubbed “magnetic sponges” by Kahn et al. many years ago.<sup>5a</sup> Also of relevance is the discovery by Kurmoo et al., who reported a minimal change of framework geometry of ca. 0.5 vol % of a nanoporous material, [Co<sup>III</sup>(OH)<sub>2</sub>(C<sub>4</sub>O<sub>4</sub>)<sub>2</sub>]·3H<sub>2</sub>O, effected by the loss of water molecules with heating up to ca. 200 °C that induces a drastic magnetic change from ferromagnetic/antiferromagnetic at temperatures between 6 and 8 K.<sup>5d</sup> These magnetic changes are attributed to the presence or loss of hydrogen bonding related to interstitial water molecules that mediate weak antiferromagnetic exchange interactions between the ferromagnetic sublattices. Another recent example of solvent-induced magnetic properties is the report by Dunbar et al., where removal of methanol molecules from the interstices of a metal–organic framework based on a two-dimensional (2D) hexagonal Mn<sup>II</sup>-TCNQF<sub>4</sub> net (TCNQF<sub>4</sub> = 2,3,5,6-tetrafluoro-7,7,8,8-tetracyanoquinodimethane) results in a conversion from weak antiferromagnetic to ferromagnetic coupling, which leads to the formation of a glassy magnet; the magnetic behavior can be reversibly cycled between the solvated and desolvated forms of the material by heating and immersion in methanol.<sup>5g</sup>

Herein we report a new 2D layered compound, [{Ru<sub>2</sub>(O<sub>2</sub>CPh-*o*-Cl)<sub>4</sub>]<sub>2</sub>TCNQ(OMe)<sub>2</sub>]·CH<sub>2</sub>Cl<sub>2</sub> (**1**), composed of a 2:1 ratio of

- (2) (a) Coronado, E.; Giménez-López, M. C.; Levchenko, G.; Romero, F. M.; García-Baonza, V.; Milner, A.; Paz-Pasternak, M. *J. Am. Chem. Soc.* **2005**, *127*, 4580. (b) Egan, L.; Kamenev, K.; Papanikolaou, D.; Takabayashi, Y.; Margadonna, S. *J. Am. Chem. Soc.* **2006**, *128*, 6034. (c) Ohba, M.; Kaneko, W.; Kitagawa, S.; Maeda, T.; Mito, M. *J. Am. Chem. Soc.* **2008**, *130*, 4475.
- (3) Sato, O.; Iyoda, T.; Fujishima, A.; Hashimoto, K. *Science* **1996**, *271*, 49.
- (4) Ohkoshi, S.; Arai, K.; Sato, Y.; Hashimoto, K. *Nat. Mater.* **2004**, *3*, 857.
- (5) (a) Larionova, J.; Chavan, S. A.; Yakhmi, J. V.; Frøystein, A. G.; Sletten, J.; Sourisseau, C.; Kahn, O. *Inorg. Chem.* **1997**, *36*, 6374. (b) Maspoeh, D.; Ruiz-Molina, D.; Wurst, K.; Domingo, N.; Cavallini, M.; Biscarini, F.; Tejada, J.; Rovira, C.; Veciana, J. *Nat. Mater.* **2003**, *2*, 190. (c) Kurmoo, M.; Kumagai, H.; Hughes, S. M.; Kepert, C. J. *Inorg. Chem.* **2003**, *42*, 6709. (d) Kurmoo, M.; Kumagai, H.; Chapman, K. W.; Kepert, C. J. *Chem. Commun.* **2005**, 3012. (e) Yanai, N.; Kaneko, W.; Yoneda, K.; Ohba, M.; Kitagawa, S. *J. Am. Chem. Soc.* **2007**, *129*, 3496. (f) Milon, J.; Daniel, M.-C.; Kaiba, A.; Guionneau, P.; Brandés, S.; Sutter, J.-P. *J. Am. Chem. Soc.* **2007**, *129*, 13872. (g) Lopez, N.; Zhao, H.; Prosvirin, A. V.; Chouai, A.; Shatrak, M.; Dunbar, K. R. *Chem. Commun.* **2007**, 4611. (h) Cheng, X.-N.; Zhang, W.-X.; Chen, X.-M. *J. Am. Chem. Soc.* **2007**, *129*, 15738. (i) Ohkoshi, S.; Tsunobuchi, Y.; Takahashi, H.; Hozumi, T.; Shiro, M.; Hashimoto, K. *J. Am. Chem. Soc.* **2007**, *129*, 3084. (j) Zhang, Y.-J.; Liu, T.; Kanegawa, S.; Sato, O. *J. Am. Chem. Soc.* **2009**, *131*, 7942. (k) Duan, Z.; Zhang, Y.; Zhang, B.; Zhu, D. *J. Am. Chem. Soc.* **2009**, *131*, 6934.
- (6) (a) Kaneko, W.; Ohba, M.; Kitagawa, S. *J. Am. Chem. Soc.* **2007**, *129*, 13706. (b) Ghosh, S. K.; Kaneko, W.; Kiriya, D.; Ohba, M.; Kitagawa, S. *Angew. Chem., Int. Ed.* **2008**, *47*, 8843.
- (7) (a) Kosaka, W.; Nomura, K.; Hashimoto, K.; Ohkoshi, S. *J. Am. Chem. Soc.* **2005**, *127*, 8590. (b) Nihei, M.; Han, L.; Oshio, H. *J. Am. Chem. Soc.* **2007**, *129*, 5312. (c) Neville, S. M.; Halder, G. J.; Chapman, K. W.; Duriska, M. B.; Southon, P. D.; Cashion, J. D.; Létard, J.-F.; Moubaraki, B.; Murray, K. S.; Kepert, C. J. *J. Am. Chem. Soc.* **2008**, *130*, 2869. (d) Ohba, M.; Yoneda, K.; Agustí, G.; Muñoz, M. C.; Gaspar, A. B.; Real, J. A.; Yamasaki, M.; Ando, H.; Nakao, Y.; Sakaki, S.; Kitagawa, S. *Angew. Chem., Int. Ed.* **2009**, *48*, 4767. (e) Neville, S. M.; Halder, G. J.; Chapman, K. W.; Duriska, M. B.; Moubaraki, B.; Murray, K. S.; Kepert, C. J. *J. Am. Chem. Soc.* **2009**, *131*, 12106.
- (8) (a) Shimamoto, N.; Ohkoshi, S.; Sato, O.; Hamshimoto, K. *Inorg. Chem.* **2002**, *41*, 678. (b) Tokoro, H.; Ohkoshi, S.; Matsuda, T.; Hashimoto, K. *Inorg. Chem.* **2004**, *43*, 5231. (c) Ohkoshi, S.; Matsuda, T.; Tokoro, H.; Hashimoto, K. *Chem. Mater.* **2005**, *17*, 81. (d) Ohkoshi, S.; Ikeda, S.; Hozumi, T.; Kashiwagi, T.; Hashimoto, K. *J. Am. Chem. Soc.* **2006**, *128*, 5320.

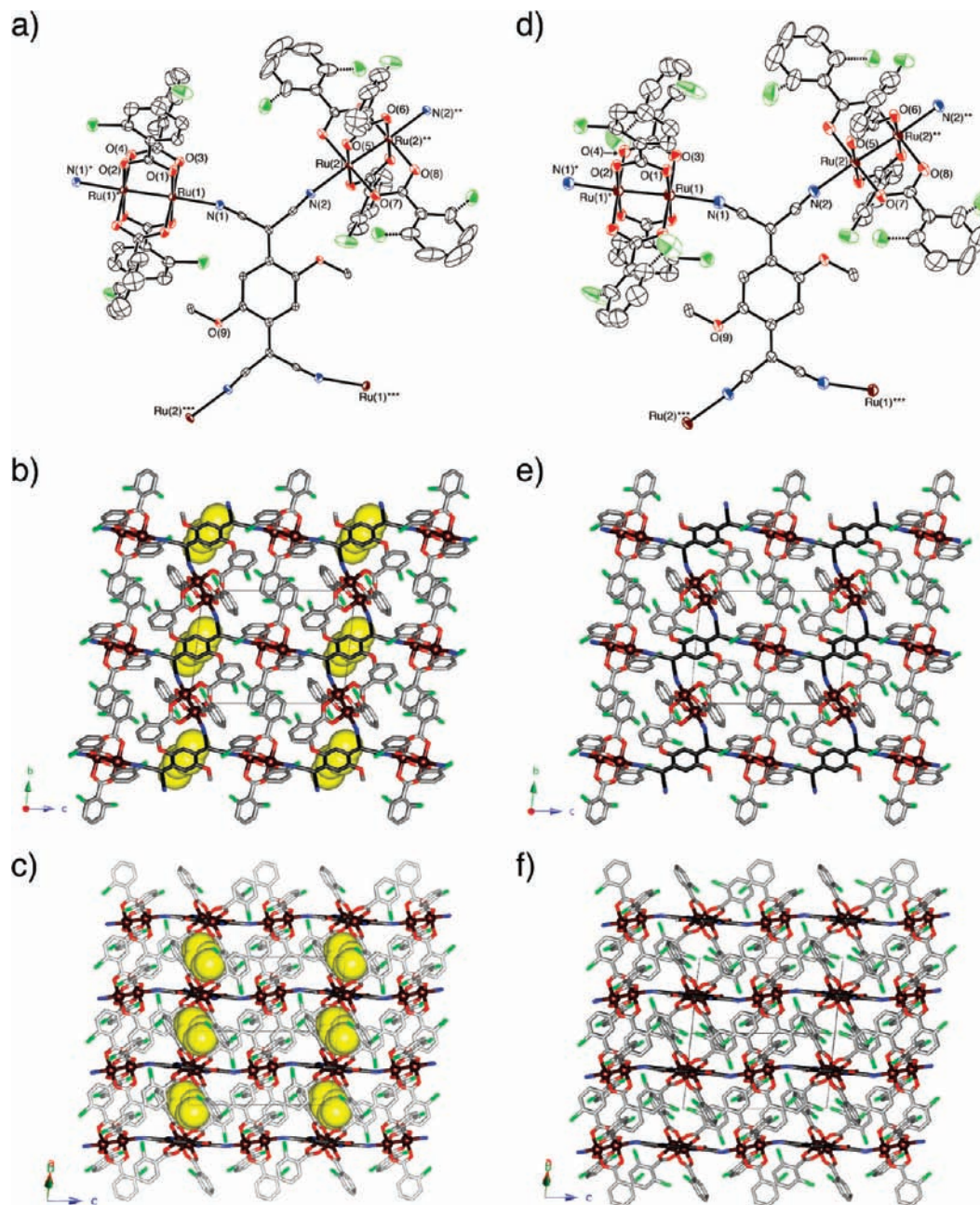
the paddlewheel diruthenium unit [Ru<sub>2</sub><sup>II,III</sup>(O<sub>2</sub>CPh-*o*-Cl)<sub>4</sub>] (*o*-CIPhCO<sub>2</sub><sup>-</sup> = *o*-chlorobenzoate) and 2,5-dimethoxy-7,7,8,8-tetracyanoquinodimethane (TCNQ(MeO)<sub>2</sub>) and one molecule of CH<sub>2</sub>Cl<sub>2</sub> located between layers. Reversible magnetism between antiferromagnetic and ferromagnetic is extremely sensitive to the solvation/desolvation of the crystallization solvent (CH<sub>2</sub>Cl<sub>2</sub>) at room temperature. This material is different from the aforementioned cases in that the gradual magnetic change occurs without significant lattice deformation or magnetic path cleavage or path formation of hydrogen bonds but is instead associated with slight structural fluctuations caused by the ordering/disordering of ligand orientation driven by the fix-and-release of the CH<sub>2</sub>Cl<sub>2</sub> molecules acting as a clip. In the case of partially desolvated crystals that have mixed domains of ferromagnetically and antiferromagnetically ordered domains for desolvated and solvated segments, respectively, the complete change to a ferromagnet can also be triggered by magnetic fields even if the desolvated segments are minor as compared to the solvated segments in a crystal. Surprisingly, the information of the existence of ferromagnetically ordered domains is dynamically recorded in the entire crystal after applying significant magnetic fields as if the majority of the antiferromagnetically ordered domains were never present.

## Results and Discussion

Compound **1** was prepared by a slow diffusion reaction of [Ru<sub>2</sub>(O<sub>2</sub>CPh-*o*-Cl)<sub>4</sub>(THF)<sub>2</sub>]<sup>9</sup> in CH<sub>2</sub>Cl<sub>2</sub> (bottom layer) and TCNQ(OMe)<sub>2</sub> in nitrobenzene (top layer) under an ultrapure N<sub>2</sub> atmosphere. Dark-green block-shaped crystals of **1** were obtained, which crystallized in the triclinic space group *P*-1 (*Z* = 1). There are two different [Ru<sub>2</sub>] units, [Ru(1)<sub>2</sub>] and [Ru(2)<sub>2</sub>], and one TCNQ(OMe)<sub>2</sub> molecule in the formula unit (Figure 1a) with the [Ru<sub>2</sub>] units and TCNQ(MeO)<sub>2</sub> being situated on inversion centers at the midpoint of the Ru–Ru bond and the quinonoid ring of TCNQ(MeO)<sub>2</sub>, where only [Ru(2)<sub>2</sub>] has a positional disorder in its *o*-CIPh groups (vide infra). The [Ru<sub>2</sub>] and TCNQ(MeO)<sub>2</sub> units act as a linear-coordination acceptor and a μ<sub>4</sub>-bridging ligand (coordination-donor), respectively, the result of which is a fishnet-like hexagonal 2D network (Figure 1b). Relevant metrical parameters are Ru–N≡C [Ru(1)–N(1) = 2.221(3) Å, Ru(2)–N(2) = 2.236(3) Å, Ru(1)–N(1)–C(29) = 160.6(3)°, Ru(2)–N(2)–C(31) = 165.2(3)°] (Table 1). The interlayer distance, defined as the distance between the least-squares planes of the 2D sheets, is 8.367 Å. One CH<sub>2</sub>Cl<sub>2</sub> molecule of crystallization is located between the layers (Figure 1c).

The oxidation state of the molecules in the extended structure can be roughly estimated from characteristic bonds. For the [Ru<sub>2</sub>] unit, Ru–O<sub>eq</sub> (O<sub>eq</sub> = carboxylate oxygen) distances reflect the valence of [Ru<sub>2</sub>] unit; for comparison sake, we note that average values for [Ru<sub>2</sub><sup>II,III</sup>(O<sub>2</sub>CPh-*o*-Cl)<sub>4</sub>(THF)<sub>2</sub>]·2THF and [Ru<sub>2</sub><sup>II,III</sup>(O<sub>2</sub>CPh-*o*-Cl)<sub>4</sub>(THF)<sub>2</sub>]BF<sub>4</sub>·THF are 2.065 and 2.019 Å, respectively (Table S1 and Figure S1 in Supporting Information).<sup>9</sup> The average corresponding distances in **1** are 2.036 and 2.044 Å for the [Ru(1)<sub>2</sub>] and [Ru(2)<sub>2</sub>] units, respectively, values that are intermediate between those for [Ru<sub>2</sub><sup>II,II</sup>] and [Ru<sub>2</sub><sup>II,III</sup>]. These data are an indication of the occurrence of charge transfer to TCNQ(MeO)<sub>2</sub> with the result formally being [Ru<sub>2</sub><sup>4.5+</sup>] units.

(9) The starting material for **1**, [Ru<sub>2</sub><sup>II,III</sup>(O<sub>2</sub>CPh-*o*-Cl)<sub>4</sub>(THF)<sub>2</sub>]·2THF, and its oxidized material, [Ru<sub>2</sub><sup>II,III</sup>(O<sub>2</sub>CPh-*o*-Cl)<sub>4</sub>(THF)<sub>2</sub>]BF<sub>4</sub>·THF, were synthesized following general methods reported previously and crystallographically characterized (Table S1 and Figure S1 in Supporting Information and CCDC-770525 and 770524, respectively).



**Figure 1.** Thermal ellipsoid plots of the formula unit of **1** (a) and **1-dry** (d) (50% probability ellipsoids; symmetry operations (\*)  $1 - x, 2 - y, -z$ ; (\*\*)  $2 - x, 1 - y, 1 - z$ ; (\*\*\*)  $2 - x, 1 - y, -z$ ), where disordered Cl atoms of the  $[Ru_2]$  moiety are represented by dashed bonds, and packing diagrams are projected along the  $a$  axis (b) and (e) and the  $[1-10]$  direction (c) and (f) for **1** and **1-dry**, respectively. The  $CH_2Cl_2$  molecules in **1** are represented by a yellow CPK model. Hydrogen atoms are omitted for the sake of clarity.

The bond distances in  $TCNQ(MeO)_2$  are also sensitive to the charge that varies from the quinonoid (neutral) form with  $TCNQ(MeO)_2^0$  to the benzenoid (ionic) form with  $TCNQ(MeO)_2^{\cdot-}$ . The charge was estimated on the basis of the Kistenmacher relationship  $\rho = A[c/(b + d)] + B$  with  $A_H = -41.667$  and  $B_H = 19.833$  for the original  $TCNQ$ ,<sup>10</sup> where  $b$ ,  $c$ , and  $d$  are respective bond distances for 7,9-, 1,7-, and 1,2-positioned C–C sets in the  $TCNQ(MeO)_2$  moiety of **1** (see Table 1).<sup>11</sup> The estimated  $\rho$  value for **1** is  $-1.50$ , which in accord with a charge balance of  $\{[Ru_2^{4.5+}] - TCNQ(MeO)_2^{\cdot-} - [Ru_2^{4.5+}]\}$

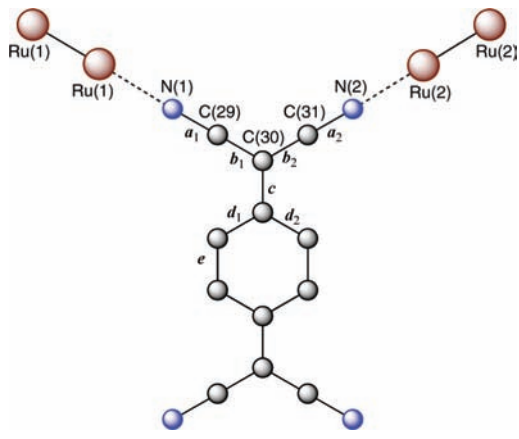
as reported previously for  $\{[Ru_2(O_2CCF_3)_4]_2TCNQF_4\} \cdot 3(p\text{-xylene})$  ( $CF_3CO_2^-$  = trifluoroacetate,  $TCNQF_4$  = 2,3,5,6-tetrafluoro-7,7,8,8-tetracyanoquinodimethane).<sup>12</sup>

IR data for **1** also support the assignment of the oxidation state. The  $\nu(C\equiv N)$  modes for  $TCNQ(MeO)_2$  appear at 2193, 2157, and 2106  $cm^{-1}$  for **1**, which supports the assignment of the radical anion form of the  $TCNQ(OMe)_2$  moiety because of significant red-shifting as compared to neutral  $TCNQ(OMe)_2^0$

(10) Kistenmacher, T. J.; Emge, T. J.; Bloch, A. N.; Cowan, D. O. *Acta Crystallogr., Sect. B* **1982**, *38*, 1193.

(11) Miyasaka, H.; Campos-Fernández, C. S.; Clérac, R.; Dunbar, K. R. *Angew. Chem., Int. Ed.* **2000**, *39*, 3831.

(12) (a) Miyasaka, H.; Izawa, T.; Takahashi, N.; Yamashita, M.; Dunbar, K. R. *J. Am. Chem. Soc.* **2006**, *128*, 11358. (b) Miyasaka, H.; Motokawa, N.; Matsunaga, S.; Yamashita, M.; Sugimoto, K.; Mori, T.; Toyota, N.; Dunbar, K. R. *J. Am. Chem. Soc.* **2010**, *132*, 1532.

**Table 1.** Important Bond Distances and Angles for **1**, **1-dry**, and **1'**


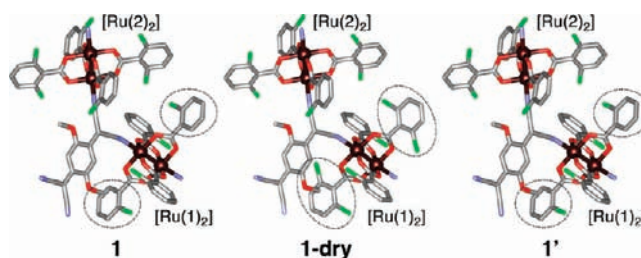
	<b>1</b>	<b>1-dry</b>	<b>1'</b>
Distances (Å)			
Ru(1)–Ru(1)	2.2778(4)	2.2723(5)	2.2750(4)
Ru(2)–Ru(2)	2.2835(4)	2.2796(4)	2.2812(4)
Ru(1)–O(1)	2.020(3)	2.019(3)	2.021(3)
Ru(1)–O(2)	2.042(3)	2.037(3)	2.041(3)
Ru(1)–O(3)	2.037(3)	2.025(3)	2.035(3)
Ru(1)–O(4)	2.043(3)	2.034(3)	2.045(3)
Ru(2)–O(5)	2.043(3)	2.037(3)	2.040(3)
Ru(2)–O(6)	2.040(3)	2.033(3)	2.044(3)
Ru(2)–O(7)	2.040(3)	2.040(3)	2.040(3)
Ru(2)–O(8)	2.054(3)	2.046(3)	2.049(3)
Ru(1)–N(1)	2.221(3)	2.207(4)	2.214(3)
Ru(2)–N(2)	2.236(3)	2.225(4)	2.235(3)
$a_1, a_2$	1.157(5), 1.150(5)	1.148(6), 1.136(6)	1.158(5), 1.138(6)
$b_1, b_2$	1.395(5), 1.410(5)	1.410(6), 1.407(7)	1.395(6), 1.406(6)
$c$	1.441(5)	1.430(7)	1.455(6)
$d_1, d_2$	1.410(5), 1.413(5)	1.408(7), 1.419(6)	1.405(6), 1.400(6)
$e$	1.382(6)	1.373(7)	1.388(6)
Angles (deg)			
Ru(1)–Ru(1)–N	177.40(10)	175.86(11)	177.38(10)
Ru(2)–Ru(2)–N	175.69(9)	174.80(11)	175.72(19)
Ru(1)–N(1)–C(29)	160.6(3)	161.1(4)	161.1(3)
Ru(2)–N(2)–C(31)	165.2(3)	161.9(4)	165.4(3)

(2219  $\text{cm}^{-1}$ ). As a point of reference, the IR stretches in the  $\nu(\text{C}\equiv\text{N})$  region for LiTCNQ(OMe)<sub>2</sub> are located at 2196 and 2173  $\text{cm}^{-1}$ .

Compound **1** gradually releases  $\text{CH}_2\text{Cl}_2$  molecules at room temperature under a  $\text{N}_2$  atmosphere without loss of crystallinity to form a stable  $\text{CH}_2\text{Cl}_2$ -free compound (**1-dry**) after 24 h or more (**1-dry** can also be obtained by heating at 150 °C for 30 min but would have many more defects than samples prepared at ambient temperatures). Remarkably, single-crystal X-ray analysis of **1-dry** (Figure 1d–f) revealed no significant changes in lattice dimensions and a volume change of 1.2 vol % (see Experimental Section). The only notable change is a disorder in the orientation of two *o*-CIPh groups of the  $[\text{Ru}(1)_2]$  moiety (Table 1 and Figure 2).<sup>13</sup> This order/disorder of the *o*-CIPh groups appears to be a key element in dictating the magnetic modifications (vide infra). Furthermore, **1-dry** absorbs  $\text{CH}_2\text{Cl}_2$  reversibly to revert with near completion back to the original compound **1** after being exposed to  $\text{CH}_2\text{Cl}_2$  vapor for 72 h (distinguished as **1'**).<sup>14</sup> Compound **1'** was also crystallographi-

(13) The average Ru–O<sub>eq</sub> distances for  $[\text{Ru}(1)_2]$  and  $[\text{Ru}(2)_2]$  in **1-dry** are 2.029 and 2.039 Å, which correspond to the quasi- $[\text{Ru}_2^{4.5+}]$  state as well as **1**. The  $r$  value of TCNQ(MeO)<sub>2</sub> for **1-dry** estimated using the Kistenmacher relationship is  $-1.28$ .

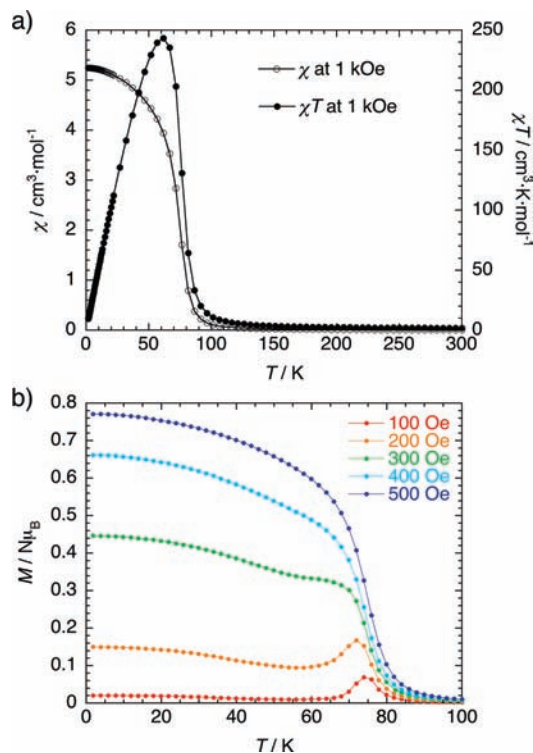
(14) The average Ru–O<sub>eq</sub> distances for  $[\text{Ru}(1)_2]$  and  $[\text{Ru}(2)_2]$  in **1'** are 2.036 and 2.043 Å, which correspond to the quasi- $[\text{Ru}_2^{4.5+}]$  state as well as **1**. The  $\rho$  value of TCNQ(MeO)<sub>2</sub> for **1'** is  $-1.80$ .



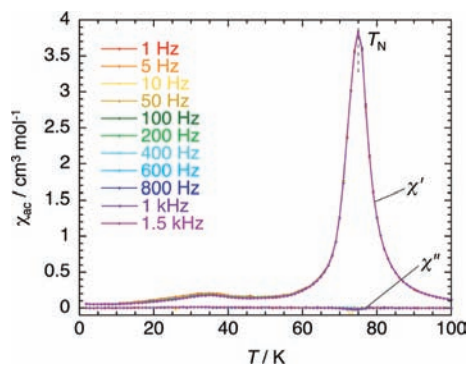
**Figure 2.** Visualization of the variation in the formula unit via the process of desolvation/solvation (from left, **1**, **1-dry**, and **1'**), in which dashed circles indicate an order/disorder in the *o*-CIPh group of the  $[\text{Ru}(1)_2]$  moiety concomitant with changes in solvation.

cally characterized to confirm that nearly 100% of the  $\text{CH}_2\text{Cl}_2$  molecules were present (Figure S2 in Supporting Information). It should be noted that the *o*-CIPh groups of  $[\text{Ru}(1)_2]$  of **1'**, which were disordered in **1-dry**, become ordered again as **1**, whereas those of  $[\text{Ru}(2)_2]$  remain disordered through the entire process of **1**  $\rightarrow$  **1-dry**  $\rightarrow$  **1'** (Figure 2). Important bond distances and angles of **1'** are listed in Table 1. No significant difference is observed among the series. The charge distribution in the change from **1**  $\rightarrow$  **1-dry**  $\rightarrow$  **1'** is essentially invariant: The average Ru–O<sub>eq</sub> distances for the  $[\text{Ru}(1)_2]$  and  $[\text{Ru}(2)_2]$  units are 2.029 and 2.039 Å in **1-dry** and 2.036 and 2.043 Å in **1'**, being intermediate between values for  $[\text{Ru}_2^{\text{II,II}}]$  and  $[\text{Ru}_2^{\text{II,III}}]$  as well as **1**, and the  $\rho$  value estimated from the TCNQ(MeO)<sub>2</sub> moiety using the Kistenmacher relationship is  $-1.28$  and  $-1.80$  for **1-dry** and **1'**, respectively. The lack of oxidation state conversion in going from **1**  $\rightarrow$  **1-dry**  $\rightarrow$  **1'** was also confirmed by solid state diffuse reflectance spectra of these compounds (Figure S3 in Supporting Information), in which three important bands, the  $\pi$ – $\pi^*$  band of TCNQ(MeO)<sub>2</sub><sup>•–</sup> at ca. 1.5 eV, the charge-transfer band of  $[\text{Ru}_2^{\text{II,III}}] \rightarrow \text{TCNQ}(\text{MeO})_2$  at ca. 0.8 eV, and the intervalence charge-transfer band between  $[\text{Ru}_2^{\text{II,II}}]$  and  $[\text{Ru}_2^{\text{II,III}}]^+$  at energies less than 0.8 eV, were continuously observed throughout the series.

Field-cooled dc magnetic susceptibility (FCM) data were collected on a freshly harvested polycrystalline sample of **1** in the temperature range of 1.8–300 K at several fields (Figure 3). The  $\chi T$  value of  $1.80 \text{ cm}^3 \cdot \text{K} \cdot \text{mol}^{-1}$  at 300 K (at 1 kOe; Figure 3a) is less than the spin-only value of  $2.00 \text{ cm}^3 \cdot \text{K} \cdot \text{mol}^{-1}$  for a set of two  $S = 1$  spins with  $g = 2.00$  for isolated  $[\text{Ru}_2^{\text{II,II}}]$  units as calculated on the basis of no redox reaction. This result not only indicates that the charge transfer from the  $[\text{Ru}_2^{\text{II,II}}]$  unit to the TCNQ(MeO)<sub>2</sub> moiety occurs in **1** but also that a significant coupling of magnetic centers occurs through TCNQ(MeO)<sub>2</sub><sup>•–</sup> within and between layers even at high temperatures (vide infra). The observed lower  $\chi T$  values at high temperatures are attributed to the following three reasons. The first is the large anisotropy of  $[\text{Ru}_2^{\text{II,II}}]$  and  $[\text{Ru}_2^{\text{II,III}}]$  units with  $D \approx 400$  K ( $S = 1$ ) and  $D \approx 100$  K ( $S = 3/2$ ), respectively. The second one is that antiferromagnets (such as **1**; vide infra) in this type of system have strong interlayer antiferromagnetic interactions even at high temperatures (vide infra).<sup>12</sup> The last one is that it is not obvious whether the spin arrangement in a layer is ferromagnetic or ferrimagnetic because of the above two reasons. Upon decreasing the temperature, the  $\chi T$  value gradually increases in the high temperature region and then drastically increases at around 80 K to reach  $243 \text{ cm}^3 \cdot \text{K} \cdot \text{mol}^{-1}$  at 62 K followed by a decrease to  $9.50 \text{ cm}^3 \cdot \text{K} \cdot \text{mol}^{-1}$  at 1.8 K. As expected from this  $\chi T$  behavior, the  $\chi$  value at 1 kOe exhibits a rapid increase at ca. 80 K without any decrease being observed over the entire temperature range (Figure 3a). Measurements

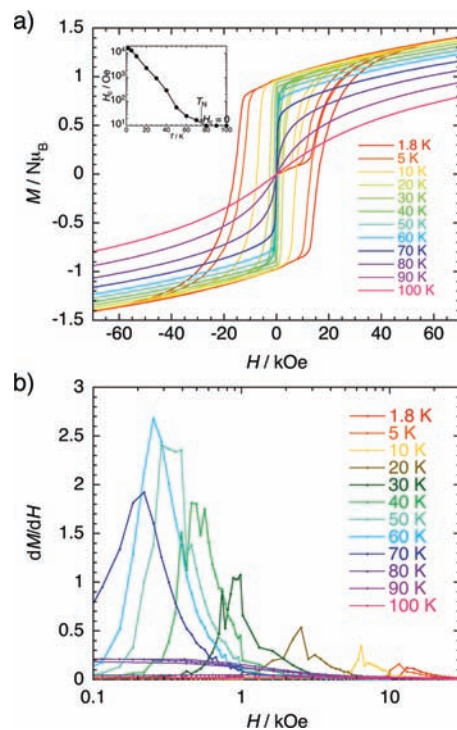


**Figure 3.** Temperature dependence of  $\chi$  and  $\chi T$  measured at 1 kOe (a) and field-cooled magnetization curves measured under different external fields less than 1 kOe for **1** (b). The solid line is a guide for the eye.

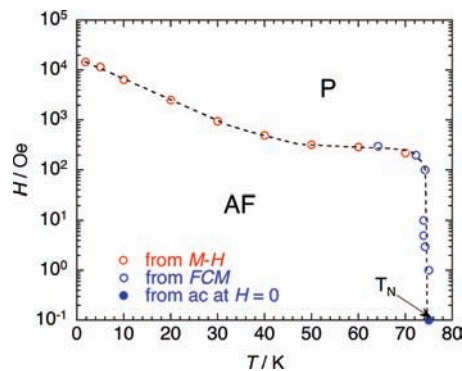


**Figure 4.** Temperature dependence of the ac susceptibilities  $\chi'$  (in-phase) and  $\chi''$  (out-of-phase) of **1** at zero dc field and in a 3 Oe ac oscillating field.

at an external field less than 300 Oe, however, show a peak around 70–75 K (Figure 3b), owing to a spin flip from an antiferromagnetic (AF) phase to a paramagnetic (P) phase. To obtain more details of the spin ordering near this temperature, temperature dependence of the ac susceptibility was measured under a zero dc field and a 3 Oe oscillating field. The in-phase susceptibility ( $\chi'$ ) shows a sharp peak at 75 K without frequency dependence (Figure 4), and there is no anomaly in the out-of-phase susceptibility ( $\chi''$ ), indicating the occurrence of an antiferromagnetic phase transition with  $T_N = 75$  K. We note that a small, broad peak for  $\chi'$  was also observed at  $\sim 35$  K, which is due to defects caused by a minimal loss of solvent (vide infra). This spin flip phenomenon can also be observed in the field dependence of the magnetization (Figure 5a); the initial magnetization experiences a spin flip that can be detected as a peak in a  $dM/dH$  plot (Figure 5b). Ultimately, these data lead to an  $H$ – $T$  phase diagram for **1** as shown in Figure 6 characteristic of metamagnetism.<sup>15</sup> Nevertheless, this



**Figure 5.** (a) Field dependence of the magnetization measured at various temperatures between 1.8 and 100 K and (b)  $dM/dH$  vs  $H$  plots for the virgin magnetization of **1**. Inset of (a): temperature dependence of the coercive field ( $H_c$ ).

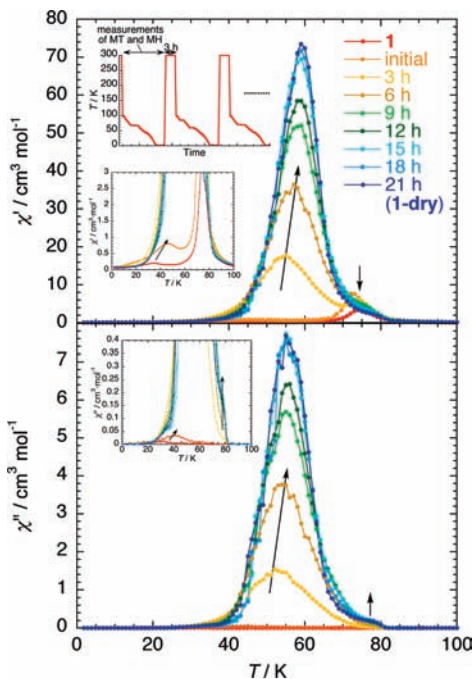


**Figure 6.**  $H$ – $T$  phase diagram for **1**, where AF and P represent the antiferromagnetic and paramagnetic phases, respectively.  $T_N$  (75 K) was determined from the  $\chi'$  versus  $T$  data at  $H = 0$  (Figure 4). The dashed line is a guide for the eye.

metamagnetic behavior is unusual; after the material achieves a P-phase, **1** becomes a field-induced canted antiferromagnet with a large coercivity up to 1.6 T at 1.8 K (Figure 5a). The coercivity disappears at ca. 80 K (inset of Figure 5a).<sup>16</sup> The details of the  $M$ – $H$  hysteresis will be described below.

The sample of **1** was gradually dried in situ in a SQUID apparatus by repeating the process of standing for 3 h at 300 K with venting followed by cooling to 100 K to measure the ac susceptibility from 100 to 1.8 K and an  $MH$  curve at 1.8 K (the time profile for the measurements is given in the inset of Figure 7). Figure 7 displays the variation of temperature dependence of ac susceptibilities (1 Hz) as the process is repeated 8 times

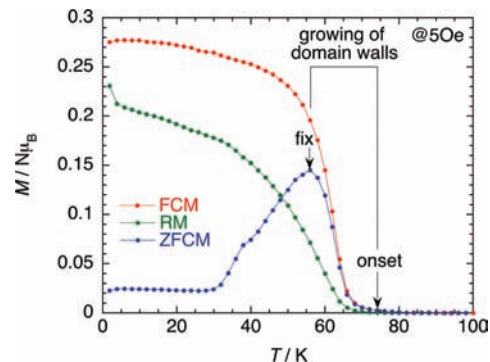
(15) Considering the small  $\chi T$  value at 300 K and the value of the saturation magnetization in  $M$  vs  $H$  plots, the P-phase for **1** may be associated with a spin canted mode. The spin flop (SF) phase was not detected in measurements performed in this work.



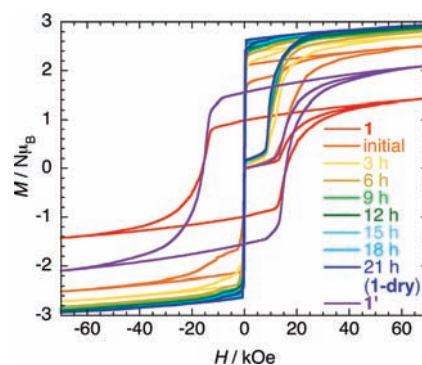
**Figure 7.** Variation of 1 Hz ac susceptibilities  $\chi'$  (top) and  $\chi''$  (bottom) (zero dc field and 3 Oe ac oscillating field) during an in situ desolvation process, where the times in the legend represent integrated times at 300 K (each step has a holding time of 3 h, as the time profile indicates in the inset). Detailed views of the initial data and after 3 h are also shown in the inset.

(ultimately, the sample was kept for 21 h at 300 K). As the process of desolvation proceeds, the peak in  $\chi'$  at 75 K ( $= T_N$ ) for **1** decreases and a new maximum in  $\chi'$  appears in the range 50–60 K with a distinct signal being observed in  $\chi''$ . This new feature appears to be a result of a shift in the broad anomaly peak at 35 K observed in **1** (inset of Figure 5; it is therefore concluded that the broad peak in **1** is a result of defects associated with the desolvation). Whereas this peak is finally saturated after 21 h at 300 K, conversely, the  $\chi'$  feature at 75 K that disappeared after 9 h at 300 K reappears and increases along with the appearance of a  $\chi''$  signal.

The aforementioned results are interpreted as follows: The  $\chi'$  maximum at 50–60 K represents a spontaneous magnetization that involves a fixing of the ferromagnetically ordered domains with a  $\chi''$  signal that begins to appear at ca. 75 K in a gradual fashion. Such a slow increase in  $\chi''$  has often been observed for spin-glass-like materials or magnets with anisotropic spins.<sup>17,18</sup> Indeed, the present system is composed of anisotropic spins. Meanwhile, the small anomaly at 75–80 K that appeared after 21 h is probably due to the effect of some defects. To further probe this process, FCM, remnant magne-



**Figure 8.** In situ FCM, RM, and ZFCM for the in situ sample after 21 h (corresponding to **1-dry**), where a field of 5 Oe was applied for FCM and ZFCM.



**Figure 9.** Field dependence of the magnetization at 1.8 K for **1**, the samples produced in the in situ desolvation process, and **1'**.

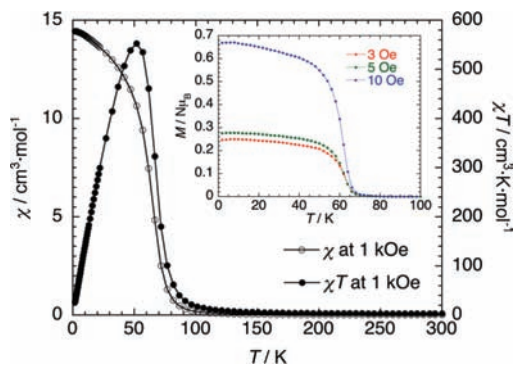
tization (RM), and zero-field-cooled magnetization (ZFCM) were measured for the in situ sample after 21 h (i.e., corresponding to **1-dry**) at 5 Oe (Figure 8). The ZFCM leads to a peak at 56 K, in good agreement with the ac data, but completely follows FCM above 75 K. In addition, RM disappears at this temperature. These data are in accord with the conclusion of a gradual growth of ferromagnetically ordered domains, a process that begins at ca. 75 K and fixes at 56 K.<sup>19</sup>

The  $M$  versus  $T$  data for our new material indicate that, with gradual elimination of the  $\text{CH}_2\text{Cl}_2$  solvent of crystallization at room temperature, the magnetic properties of the present compound are tuned from an antiferromagnet for **1** to a ferromagnet for **1-dry**, with intermediate species being possible wherein both domains are present as mixtures.

Field dependence of the magnetization of all in situ samples was measured at 1.8 K (Figure 9) immediately following the measurements of the ac data (Figure 7) and  $M$  versus  $T$  data (Figure 8). For a fresh sample of **1**, the initial magnetization curve indicates a flip at 1.5 T to transfer to the P-phase and reaches  $M_s = 1.43 \mu_B$  at 7 T, showing a metamagnetic transition typically observed for anisotropic antiferromagnets. Interestingly, this saturated magnetization does not follow the initial process and results in a magnetization at zero field (remnant magnetization) and a field-dependent hysteresis with a coercivity of  $H_c = 1.6$  T; these data represent that of a field-induced canted-antiferromagnet (Figures 5 and 9). Such a large coercivity implies a hard magnet, a result that has been reported in the literature for other 2D network compounds.<sup>12,16,20</sup> This phe-

- (16) (a) Kurmoo, M. *Philos. Trans. R. Soc.* **1999**, *357*, 3041. (b) Kurmoo, M.; Kumagai, H.; Green, M. A.; Lovett, B. W.; Blundell, S. J.; Ardavan, A.; Singleton, J. *J. Solid State Chem.* **2001**, *159*, 343. (c) Kumagai, H.; Keppert, C. J.; Kurmoo, M. *Inorg. Chem.* **2002**, *41*, 3410. (d) Kurmoo, M.; Kumagai, H.; Hugues, S. M.; Kepert, C. J. *Inorg. Chem.* **2003**, *42*, 6709. (e) Numata, Y.; Inoue, K.; Buranov, N.; Kurmoo, M.; Kikuchi, K. *J. Am. Chem. Soc.* **2007**, *129*, 9902. (f) Ishii, N.; Okamura, Y.; Chiba, S.; Nogami, T.; Ishida, T. *J. Am. Chem. Soc.* **2008**, *130*, 24.
- (17) Miyasaka, H.; Nakata, K.; Lecren, L.; Coulon, C.; Nakazawa, Y.; Fujisaki, T.; Sugiura, K.; Yamashita, M.; Clérac, R. *J. Am. Chem. Soc.* **2006**, *128*, 3770.
- (18) Coronado, E.; Galán-Mascarós, J. R.; Martí-Gastaldo, C.; Ribera, A.; Palacios, E.; Castro, M.; Burriel, R. *Inorg. Chem.* **2008**, *47*, 9103.

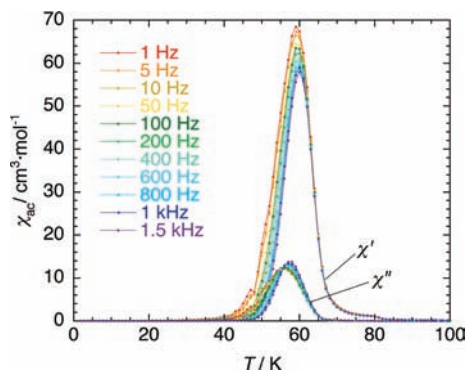
- (19) Kurmoo, M. *Chem. Soc. Rev.* **2009**, *38*, 1353.
- (20) Motokawa, N.; Oyama, T.; Matsunaga, S.; Miyasaka, H.; Yamashita, M.; Dunbar, K. R. *CrystEngComm* **2009**, *11*, 2121.



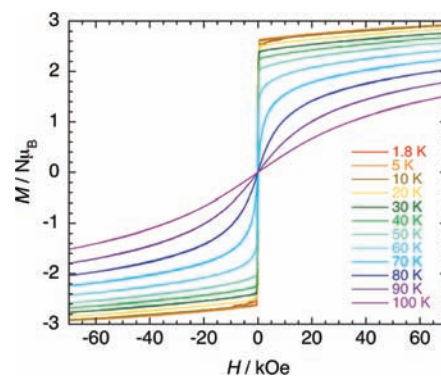
**Figure 10.** Temperature dependence of  $\chi$  and  $\chi T$  of **1-dry** produced in the in situ process (after 21 h) measured at 1 kOe. Inset: field-cooled magnetization curves measured under low external fields. The solid line is a guide for the eye.

nomenon is due to domain-wall triggers associated with the origin of interlayer antiferromagnetic interactions (between layers of solvated segments) rather than intralayer triggers such as large anisotropy arising from the  $[\text{Ru}_2]$  units. It should be pointed out that this coercivity for **1** disappears even when the sample is left for several minutes at room temperature. The initial magnetization of partially dried and **1-dry** samples still display features of a hard magnet: a spin flip is observed at 1 T. Nevertheless, the saturated magnetization becomes much higher than that observed for the fresh sample **1**, reaching  $M_s = 2.5 \mu_B$  at 7 T (with release of  $\text{CH}_2\text{Cl}_2$  the saturated magnetization gradually increases, which is most likely due to small areas of canted spin domains). Even in partially dried samples (and **1-dry**) the remnant magnetization is preserved until close to  $H = 0$  but with no coercivity; therefore these materials are basically identical soft-ferromagnets (note that butterfly-type hysteresis loops are observed at low fields in partially dried samples, which become more narrow with increasing degree of desolvation). This phenomenon is akin to a magnetic avalanche.<sup>21</sup> It should be emphasized that, even in the case of a small loss of  $\text{CH}_2\text{Cl}_2$ , which would create only a small fraction of ferromagnetically ordered domains in a crystal as observed from the ac data in Figure 7, the information of the minor segments of the ferromagnetically ordered domain dictates the state of the magnetism after the P-phase is reached in applied fields. This is quite unusual and very interesting because despite the fact that the desolvation process is expected to increase the number of defects generally capable of acting as areas of pinning for domain walls, the domain walls are easy to move in this system.

Figure 10 shows  $\chi$  and  $\chi T$  plots for **1-dry** estimated from FCM data at 1 kOe as a function of temperature. At an external field of 1 kOe, the behavior is very similar to what was found for **1** (Figure 3a), but the behavior at low fields is completely different from that of the antiferromagnet **1** (Figure 8 and inset of Figure 10). There is no flip of spins from the AF-phase to the P-phase and the  $\chi T$  value at 300 K is  $3.06 \text{ cm}^3 \cdot \text{K} \cdot \text{mol}^{-1}$ , larger than the value observed for **1**. Assuming that the intralayer magnetic nature of **1** is preserved in **1-dry**, this difference hints at the existence of strong interlayer antiferromagnetic interactions in **1** even at 300 K. The frequency dependence of ac susceptibilities was measured on a sample of **1-dry** under a zero dc field and a 3 Oe oscillating field (Figure 11; note that these



**Figure 11.** Temperature dependence of the ac susceptibilities  $\chi'$  (in-phase) and  $\chi''$  (out-of-phase) of **1-dry** produced in the in situ process (after 21 h) at zero dc field and in a 3 Oe ac oscillating field.

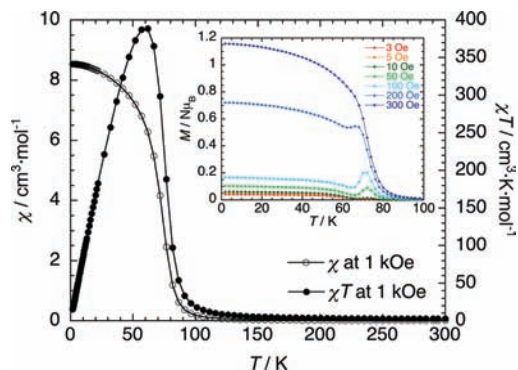


**Figure 12.** Field dependence of the magnetization of **1-dry** produced in the in situ process (after 21 h) measured at various temperatures between 1.8 and 100 K, where the initial magnetization curves are omitted for the sake of clarity.

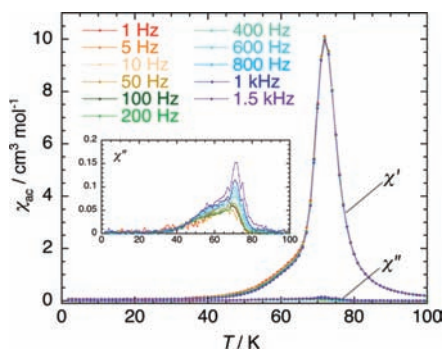
data were measured after the  $M$  vs  $H$  data.). Slight frequency dependence is observed even though the peak of  $\chi'$  is fixed, in accord with slowly growing ferromagnetically ordered domains being present as concluded from the FCM, RM, and ZFCM measurements (Figure 8). Finally,  $M$  versus  $H$  data were measured at several temperatures up to 100 K (Figure 12). The “softness” of the magnets was preserved up to 100 K after applying high fields.

The dried sample **1-dry** returns back to the solvated form of **1'** with nearly 100% occupancy for the  $\text{CH}_2\text{Cl}_2$  molecules per formula unit only by allowing the sample to stand in a  $\text{CH}_2\text{Cl}_2$  atmosphere during 72 h or more; complete conversion to **1** is not achieved at such a mild condition because of the presence of small defects. As shown in Figure 13, the spin flip phenomenon for the metamagnetic nature observed in **1** was recovered, but the  $\chi T$  value at 300 K is  $2.65 \text{ cm}^3 \cdot \text{K} \cdot \text{mol}^{-1}$  ( $1 < \mathbf{1}' < \mathbf{1-dry}$ ), which implies the presence of small defects caused by the desolvation/desolvation process rather than incomplete reversibility of solvation. Indeed, in the temperature dependence data of the ac susceptibilities, a sharp and strong maximum in  $\chi'$  was observed at 75 K, corresponding to  $T_N$ , with a broad and weak peak involving  $\chi''$  signals at 40–80 K (Figure 14). Also in the  $M$ – $H$  curve at 1.8 K, the value of  $M_s$  of **1'** is a little higher than that observed for **1**, but the coercivity is recovered to the same value as **1** (Figure 9). Thus, magnetic properties are nearly reversible between **1** and **1-dry** (the temperature dependence of  $M$ – $H$  curves and a  $H$ – $T$  phase diagram derived from the data of  $M$  vs  $T$  and  $dM$  vs  $dH$  for **1'** are provided in Figures S4 and S5, respectively, in Supporting

(21) Minguet, M.; Luneau, D.; Lhotel, E.; Villar, V.; Paulsen, C.; Amabilino, D. B.; Veciana, J. *Angew. Chem., Int. Ed.* **2002**, *41*, 586.



**Figure 13.** Temperature dependence of  $\chi$  and  $\chi T$  of  $1'$  measured at 1 kOe. Inset: field-cooled magnetization curves measured under low external fields. The solid line is a guide for the eye.



**Figure 14.** Temperature dependence of the ac susceptibilities  $\chi'$  and  $\chi''$  of  $1'$  at zero dc field and 3 Oe ac oscillating field. Inset: close-up view of  $\chi''$ .

Information). From the structural point of view, very slight changes of the interlayer environment result in a dramatic magnetic modification, although only a 1.2 vol % of volume change occurs between **1** and **1-dry**. It is proposed that the order/disorder of *o*-ClPh groups in  $[\text{Ru}(1)_2]$  is mainly responsible for tuning the magnetic properties. It is possible that the disordered form in  $[\text{Ru}(1)_2]$  results in structural/magnetic fluctuations, which not only disturb the antiferromagnetic alignment of interlayer spins but also trigger the pinning of domain walls.

## Concluding Remarks

The present compound is exquisitely sensitive to slight changes of structure that alter the magnetic properties from an antiferromagnet for  $\text{CH}_2\text{Cl}_2$ -solvated **1** at  $H = 0$  to a canted-antiferromagnet (hard magnet) under applied fields and finally to a soft ferromagnet for partially dried or dried samples (**1-dry**). The latter samples revert to a  $\text{CH}_2\text{Cl}_2$ -solvated phase (**1'**) by exposure of **1-dry** to  $\text{CH}_2\text{Cl}_2$  vapor at room temperature. Essentially, this material exhibits a robust framework with an order/disorder in a substituent group that leads to flexible magnetic ground states dependent on the degree of solvation. Thus, the present compound revealed a new concept for reversible magnetism in which a trigger as subtle as a structural fluctuation, in this case order/disorder of a ligand substituent, is crucial for deciding the magnetic properties. These results are quite different from the known cases of reversible changes in magnetism for materials that undergo major structural changes effected by interstitial solvent loss.

## Experimental Section

**Synthesis of 1.** All synthetic procedures were carried out under anaerobic conditions. The starting material  $[\text{Ru}_2(\text{O}_2\text{CPh-}o\text{-Cl})_4$ -

(THF) $_2$ ] was prepared by adaptation of a literature procedure.<sup>22</sup> A  $\text{CH}_2\text{Cl}_2$  solution (20 mL) of  $[\text{Ru}_2(\text{O}_2\text{CPh-}o\text{-Cl})_4(\text{THF})_2]$  (97 mg, 0.1 mmol) was separated into 2 mL portions and placed in narrow diameter sealed glass tubes ( $\phi = 8$  mm). Then 2 mL portions of nitrobenzene solution (20 mL) of  $\text{TCNQ}(\text{OMe})_2$  (13 mg, 0.05 mmol) were carefully placed onto the  $\text{CH}_2\text{Cl}_2$  layers to allow for slow diffusion to occur. The glass tubes were left undisturbed for 1 week or more to yield block-shaped dark-green crystals of **1**. Yield: 74%. Elemental analysis (%) calcd for  $\text{C}_{71}\text{H}_{42}\text{Cl}_{10}\text{N}_4\text{O}_{18}\text{Ru}_4$ : C 42.68, H 2.12, N 2.80. Found: C 42.90, H 2.29, N 3.05. IR (KBr):  $\nu(\text{C}\equiv\text{N})$ , 2193, 2158, 2106  $\text{cm}^{-1}$ .

**General Physical Measurements.** Infrared spectra were measured on KBr disks with a Jasco FT-IR 620 spectrophotometer. TG-DTA data for monitoring the removal of interstitial solvent molecules in the bulk preparation of **1-dry** were conducted on a Shimadzu DTG-60H instrument with a temperature sweep rate of 5 °C/min. Magnetic susceptibility measurements were conducted with a Quantum Design SQUID magnetometer (MPMS-XL) in the temperature and dc field ranges of 1.8 to 300 K and  $-7$  to 7 T. AC measurements were performed at various frequencies ranging from 1 to 1488 Hz with an ac field amplitude of 3 Oe. Polycrystalline samples embedded in liquid paraffin were measured except for the SQUID in situ preparation of **1-dry**. Experimental data were corrected for the sample holder and liquid paraffin and for the diamagnetic contribution calculated from Pascal constants.<sup>23</sup>

**Magnetic Measurements and SQUID in Situ Preparation of 1-dry.** The magnetic measurements for **1** and **1'** were first carried out using freshly prepared samples embedded in liquid paraffin to prevent the elimination of crystallization solvent ( $\text{CH}_2\text{Cl}_2$ ) under a reduced pressure. Magnetic measurements for partially dried samples prepared in situ in the SQUID were carried out by the following procedures. The freshly harvested sample of **1** in a gelatin capsule without any coating agent was put into a SQUID and immediately cooled to 100 K under reduced pressure, at which stage even the initial sample is not a fresh sample but is a partially dried sample. Ac magnetic susceptibilities and  $M-H$  curves for this sample were measured in the temperature range of 1.8–100 K, and then the sample was heated to 300 K and kept at this temperature for 3 h. This procedure was repeated (8 times) until no significant change was observed.

**Crystallography.** Single crystals with dimensions of  $0.25 \times 0.23 \times 0.04$  mm $^3$  for **1**,  $0.15 \times 0.13 \times 0.05$  mm $^3$  for **1-dry**,  $0.15 \times 0.14 \times 0.03$  mm $^3$  for **1'**,  $0.18 \times 0.16 \times 0.10$  mm $^3$  for  $[\text{Ru}_2^{\text{III}}(\text{O}_2\text{CPh-}o\text{-Cl})_4(\text{THF})_2] \cdot 2\text{THF}$ , and  $0.12 \times 0.08 \times 0.03$  mm $^3$  for  $[\text{Ru}_2^{\text{III}}(\text{O}_2\text{CPh-}o\text{-Cl})_4(\text{THF})_2]\text{BF}_4 \cdot \text{THF}$  were mounted on cryo-loops or glass fibers using Nujol and cooled by a stream of cooled  $\text{N}_2$  gas. All measurements were made on a Rigaku Saturn CCD area detector with a graphite monochromated Mo K $\alpha$  radiation ( $\lambda = 0.71070$  Å). The structures were solved by direct methods (SHELXL 97, SIR 97, and SIR 92)<sup>24</sup> or heavy-atom Patterson methods<sup>25</sup> and expanded using Fourier techniques (DIRDIF99).<sup>26</sup> Most non-hydrogen atoms in the main part of the structure were refined anisotropically, while the rest (as crystallization solvents) were

(22) Furukawa, S.; Kitagawa, S. *Inorg. Chem.* **2004**, *43*, 6464.

(23) Boudreaux, E. A.; Mulay, L. N. *Theory and Applications of Molecular Paramagnetism*; John Wiley and Sons: New York, 1976; p 491.

(24) (a) Sheldrick, G. M. *SHELXL 97*; University of Göttingen: Göttingen, Germany, 1997. (b) Altomare, A.; Burla, M.; Camballi, M.; Cascarano, G.; Giacovazzo, C.; Guagliardi, A.; Moliterni, A.; Polidori, G.; Spagna, R. *J. Appl. Crystallogr.* **1999**, *32*, 115. (c) Altomare, A.; Burla, M. C.; Camballi, M.; Cascarano, M.; Giacovazzo, C.; Guagliardi, A.; Polidori, G. *J. Appl. Crystallogr.* **1994**, *27*, 435.

(25) PATTY; Beurskens, P. T.; Admiraal, G.; Beurskens, G.; Bosman, W. P.; Garcia-Granda, S.; Gould, R. O.; Smits, J. M. M.; Smykalla, C. *The DIRDIF program system, Technical Report of the Crystallography Laboratory*; University of Nijmegen: Nijmegen, The Netherlands, 1992.

(26) DIRDIF99; Beurskens, P. T.; Admiraal, G.; Beurskens, G.; Bosman, W. P.; de Gelder, R.; Israel, R.; Smits, J. M. M. *The DIRDIF-99 Program System, Technical Report of the Crystallography Laboratory*; University of Nijmegen: Nijmegen, The Netherlands, 1999.



refined isotropically because of the presence of disorder. Hydrogen atoms were introduced as fixed contributors. Full-matrix least-squares refinements on  $F^2$  were based on observed reflections and variable parameters, and converged with unweighted and weighted agreement factors of  $R1 = \sum ||F_o| - |F_c|| / \sum |F_o|$  ( $I > 2.00\sigma(I)$ ), and  $wR2 = [\sum w(F_o^2 - F_c^2)^2 / \sum w(F_o^2)^2]^{1/2}$  (all data). All calculations were performed using the CrystalStructure crystallographic software package.<sup>27</sup> These data have been deposited as CIFs at the Cambridge Data Centre as supplementary publication nos. CCDC-769038 for **1**, 769037 for **1-dry**, 769039 for **1'**, 770525 for [Ru<sub>2</sub><sup>II,III</sup>(O<sub>2</sub>CPh-*o*-Cl)<sub>4</sub>(THF)<sub>2</sub>]**·2THF**, and 770524 for [Ru<sub>2</sub><sup>II,III</sup>(O<sub>2</sub>CPh-*o*-Cl)<sub>4</sub>(THF)<sub>2</sub>]**BF<sub>4</sub>·THF**. Copies of the data can be obtained free of charge by application to CCDC, 12 Union Road, Cambridge CB21EJ, UK (fax: (+44) 1223-336-033; email: deposit@ccdc.cam.ac.uk).

**Crystal Data for **1**.** C<sub>71</sub>H<sub>42</sub>N<sub>4</sub>O<sub>18</sub>Cl<sub>10</sub>Ru<sub>4</sub>, FW = 1997.94, triclinic *P*-1 (No. 2),  $T = 103 \pm 1$  K,  $\lambda(\text{Mo K}\alpha) = 0.71075$  Å,  $a = 10.18970(10)$  Å,  $b = 11.8946(2)$  Å,  $c = 15.8515(3)$  Å,  $\alpha = 83.299(3)^\circ$ ,  $\beta = 86.941(3)^\circ$ ,  $\gamma = 80.846(3)^\circ$ ,  $V = 1882.63(5)$  Å<sup>3</sup>,  $Z = 1$ ,  $D_{\text{calc}} = 1.762$  g·cm<sup>-3</sup>,  $F_{000} = 986.00$ ,  $2\theta_{\text{max}} = 55.0^\circ$ . Final  $R1 = 0.0467$  ( $I > 2.00\sigma(I)$ ),  $R = 0.0519$  (all data),  $wR2 = 0.1333$  (all data), GOF = 1.104 for 495 parameters and a total of 12441 reflections, 6388 unique ( $R_{\text{int}} = 0.014$ ).  $\mu = 12.132$  cm<sup>-1</sup>.  $\rho_{\text{max}} = 2.19$  e/Å<sup>3</sup> and  $\rho_{\text{min}} = -1.63$  e/Å<sup>3</sup>.

**Crystal Data for **1-dry**.** C<sub>70</sub>H<sub>40</sub>N<sub>4</sub>O<sub>18</sub>Cl<sub>8</sub>Ru<sub>4</sub>, FW = 1913.01, triclinic *P*-1 (No. 2),  $T = 103 \pm 1$  K,  $\lambda(\text{Mo K}\alpha) = 0.71075$  Å,  $a = 10.024(3)$  Å,  $b = 12.034(4)$  Å,  $c = 15.707(5)$  Å,  $\alpha = 84.078(10)^\circ$ ,  $\beta = 85.712(11)^\circ$ ,  $\gamma = 79.834(9)^\circ$ ,  $V = 1851.9(10)$  Å<sup>3</sup>,  $Z = 1$ ,  $D_{\text{calc}} = 1.715$  g·cm<sup>-3</sup>,  $F_{000} = 944.00$ ,  $2\theta_{\text{max}} = 55.0^\circ$ . Final  $R1 = 0.0485$  ( $I > 2.00\sigma(I)$ ),  $R = 0.0643$  (all data),  $wR2 = 0.1417$  (all data), GOF = 1.079 for 488 parameters and a total of 12420 reflections, 6340 unique ( $R_{\text{int}} = 0.022$ ).  $\mu = 11.595$  cm<sup>-1</sup>.  $\rho_{\text{max}} = 2.14$  e/Å<sup>3</sup> and  $\rho_{\text{min}} = -0.80$  e/Å<sup>3</sup>.

**Crystal Data for **1'**.** C<sub>71</sub>H<sub>42</sub>N<sub>4</sub>O<sub>18</sub>Cl<sub>10</sub>Ru<sub>4</sub>, FW = 1997.94, triclinic *P*-1 (No. 2),  $T = 103 \pm 1$  K,  $\lambda(\text{Mo K}\alpha) = 0.71075$  Å,  $a = 10.1872(15)$  Å,  $b = 11.8862(17)$  Å,  $c = 15.811(2)$  Å,  $\alpha = 83.433(3)^\circ$ ,  $\beta = 86.957(3)^\circ$ ,  $\gamma = 80.850(3)^\circ$ ,  $V = 1876.5(5)$  Å<sup>3</sup>,  $Z = 1$ ,  $D_{\text{calc}} = 1.768$  g·cm<sup>-3</sup>,  $F_{000} = 986.00$ ,  $2\theta_{\text{max}} = 55.0^\circ$ . Final  $R1 = 0.0518$  ( $I > 2.00\sigma(I)$ ),  $R = 0.0603$  (all data),  $wR2 = 0.1573$

(all data), GOF = 1.007 for 518 parameters and a total of 15143 reflections, 8200 unique ( $R_{\text{int}} = 0.016$ ).  $\mu = 12.172$  cm<sup>-1</sup>.  $\rho_{\text{max}} = 3.19$  e/Å<sup>3</sup> and  $\rho_{\text{min}} = -1.41$  e/Å<sup>3</sup>.

**Crystal Data for [Ru<sub>2</sub><sup>II,III</sup>(O<sub>2</sub>CPh-*o*-Cl)<sub>4</sub>(THF)<sub>2</sub>]**·2THF**.** C<sub>44</sub>H<sub>48</sub>O<sub>12</sub>Cl<sub>4</sub>Ru<sub>2</sub>, FW = 1112.81, orthorhombic *Pbca* (No. 61),  $T = 93 \pm 1$  K,  $\lambda(\text{Mo K}\alpha) = 0.71075$  Å,  $a = 9.151(4)$  Å,  $b = 20.914(10)$  Å,  $c = 23.367(18)$  Å,  $V = 4472(4)$  Å<sup>3</sup>,  $Z = 4$ ,  $D_{\text{calc}} = 1.653$  g·cm<sup>-3</sup>,  $F_{000} = 2256.00$ ,  $2\theta_{\text{max}} = 50.0^\circ$ . Final  $R1 = 0.0400$  ( $I > 2.00\sigma(I)$ ),  $R = 0.0424$  (all data),  $wR2 = 0.0938$  (all data), GOF = 1.092 for 281 parameters and a total of 28317 reflections, 3901 unique ( $R_{\text{int}} = 0.030$ ).  $\mu = 9.763$  cm<sup>-1</sup>.  $\rho_{\text{max}} = 0.80$  e/Å<sup>3</sup> and  $\rho_{\text{min}} = -0.74$  e/Å<sup>3</sup>.

**Crystal Data for [Ru<sub>2</sub><sup>II,III</sup>(O<sub>2</sub>CPh-*o*-Cl)<sub>4</sub>(THF)<sub>2</sub>]**BF<sub>4</sub>·THF**.** C<sub>40</sub>H<sub>40</sub>O<sub>11</sub>Cl<sub>4</sub>F<sub>4</sub>BRu<sub>2</sub>, FW = 1127.50, monoclinic *P*<sub>2</sub>/n (No. 14),  $T = 93 \pm 1$  K,  $\lambda(\text{Mo K}\alpha) = 0.71075$  Å,  $a = 14.8115(19)$  Å,  $b = 15.9646(19)$  Å,  $c = 18.929(2)$  Å,  $\beta = 106.6646(16)^\circ$ ,  $V = 4288.0(9)$  Å<sup>3</sup>,  $Z = 4$ ,  $D_{\text{calc}} = 1.746$  g·cm<sup>-3</sup>,  $F_{000} = 2260.00$ ,  $2\theta_{\text{max}} = 50.0^\circ$ . Final  $R1 = 0.0518$  ( $I > 2.00\sigma(I)$ ),  $R = 0.0527$  (all data),  $wR2 = 0.1220$  (all data), GOF = 1.142 for 596 parameters and a total of 26581 reflections, 7453 unique ( $R_{\text{int}} = 0.025$ ).  $\mu = 10.302$  cm<sup>-1</sup>.  $\rho_{\text{max}} = 2.67$  e/Å<sup>3</sup> and  $\rho_{\text{min}} = -1.14$  e/Å<sup>3</sup>.

**Acknowledgment.** The authors acknowledge Ms. Miho Take-mura (Tohoku University) for measurements of powder reflection spectra. This work was supported by a Grant-Aid for Scientific Research from the Ministry of Education, Culture, Sports, Science, and Technology (Japan) and The Asahi Glass Foundation (H.M.). N.M. thanks the JSPS Research Fellowships for Young Scientists for financial support. K.R.D. thanks the National Science Foundation (CHE0957840) for support of this work.

**Supporting Information Available:** X-ray crystallographic files in CIF format for **1**, **1-dry**, **1'**, [Ru<sub>2</sub><sup>II,III</sup>(O<sub>2</sub>CPh-*o*-Cl)<sub>4</sub>(THF)<sub>2</sub>]**·2THF**, and [Ru<sub>2</sub><sup>II,III</sup>(O<sub>2</sub>CPh-*o*-Cl)<sub>4</sub>(THF)<sub>2</sub>]**BF<sub>4</sub>·THF**, bond distances in [Ru<sub>2</sub><sup>II,III</sup>(O<sub>2</sub>CPh-*o*-Cl)<sub>4</sub>(THF)<sub>2</sub>]**·2THF** and [Ru<sub>2</sub><sup>II,III</sup>(O<sub>2</sub>CPh-*o*-Cl)<sub>4</sub>(THF)<sub>2</sub>]**BF<sub>4</sub>·THF**, and additional figures. This material is available free of charge via the Internet at <http://pubs.acs.org>.

JA102412G

(27) CrystalStructure 3.15: Crystal Structure Analysis Package; Rigaku and Rigaku/MS: The Woodlands, TX, 2000–2002.